SUPERCONDUCTIVITY

High-field superconducting halo in UTe_2

Sylvia K. Lewin[1,2]*†, Peter Czajka[1,2]*†, Corey E. Frank[1,2], Gicela Saucedo Salas[2], G. Timothy Noe II[3], Hyeok Yoon[2], Yun Suk Eo[2], Johnpierre Paglione[2,4], Andriy H. Nevidomskyy[5,6,7], John Singleton[3], Nicholas P. Butch[1,2]

The heavy fermion material UTe_2 is a candidate topological superconductor that exhibits multiple magnetic field–induced superconducting phases. One such phase exists only at fields greater than 40 tesla, a considerable scale given its critical temperature of only 2 K. Here, we extend measurements of this state with fields outside of the *bc* crystallographic plane and reveal its core structure: The superconducting phase wraps around the *b* axis in a halo-like fashion and appears to be stabilized by a field component perpendicular to the magnetic easy axis. This angle dependence points to a multicomponent spin-triplet order parameter with a finite angular momentum of the Cooper pairs. The pairing mechanism remains enigmatic, and UTe_2's specific magnetophilic superconducting tendencies seem incompatible with existing models for field-enhanced superconductivity.

Magnetic fields typically act to destroy superconductivity, a fact that places strict physical limitations on superconducting technologies. The heavy fermion material UTe_2 represents a notable exception to this conventional phenomenology (*1*–*4*). In addition to harboring a low-field superconducting state that is of interest for topological quantum computing applications (*5*, *6*), the material also exhibits additional superconducting phases that only exist at extraordinarily high magnetic fields, as illustrated in the full phase diagram in Fig. 1A. These include a field-reinforced state that exists up to 34 T for **H** aligned close to the UTe_2 *b* axis (*2*, *7*), as well as an even more exotic phase that has only been observed by tilting **H** ~20° to 40° from *b* toward *c* (*2*), a phase called SC_{FP}. The latter phase, which is the focus of the present study, only exists within the field-polarized (FP) state that is separated from the low-field regime by a metamagnetic transition (pink sheet in Fig. 1A).

The SC_{FP} phase only begins >40 T and persists up to at least 60 T. These field scales are particularly impressive given UTe_2's relatively low superconducting transition temperature, T_c (1.6 to 2.1 K depending on the sample) (*1*, *8*). We also emphasize that the material is fairly three-dimensional (3D) (*9*, *10*), which requires the superconductivity to be robust against orbital- and spin-based depairing mechanisms, in contrast to the numerous 2D systems for which high critical fields are only seen when **H** is directed within the conducting plane because orbital pair breaking is eliminated by their low dimensionality (*11*–*13*). It also differs from other uranium-based superconductors for which field-enhanced pairing is more straightforwardly associated with specific phase boundaries and high-symmetry directions (*14*, *15*).

[1]NIST Center for Neutron Research, National Institute of Standards and Technology, Gaithersburg, MD, USA. [2]Maryland Quantum Materials Center, Department of Physics, University of Maryland, College Park, MD, USA. [3]National High Magnetic Field Laboratory, Los Alamos National Laboratory, Los Alamos, NM, USA. [4]Canadian Institute for Advanced Research, Toronto, Ontario, Canada. [5]Department of Physics and Astronomy, Rice University, Houston, TX, USA. [6]Rice Center for Quantum Materials, Rice University, Houston, TX, USA. [7]Rice Advanced Materials Institute, Rice University, Houston, TX, USA. ***Corresponding author. Email: sylviakl@umd.edu (S.K.L.); pczajka@umd.edu (P.C.)** †These authors contributed equally to this work.

Prior experiments on the SC_{FP} phase have been limited to crystallographic planes. Superconductivity was found with magnetic fields applied in the *bc* plane (*2*, *16*), but not the *ab* plane (*2*), which has prompted speculation that there may be some special angle within the *bc* plane that permits this high-field phase (*16*). In this study, we mapped the SC_{FP} phase boundaries outside of the *bc* plane and found that SC_{FP} actually wraps around the *b* axis in a halo-like fashion (high-field blue region in Fig. 1A). Note that Figure 1A is an illustration intended to capture broad features in an extended dataset.

Measuring the transport properties of UTe_2

All measurements were performed at the National High Magnetic Field Laboratory's Pulsed Field Facility at Los Alamos National Laboratory. Data were primarily taken in a 65 T magnet system (typical field pulses were 60 T), as well as a 75 T duplex magnet (typical field pulses were 73 T). All pulses were performed at ~0.63 K unless otherwise indicated. A single-axis rotator was used, with the crystal manually placed on the sample platform such that **H** was applied at some angle θ_{bc} within the *bc* plane (Fig. 1B). Between field pulses, the rotator was used to reposition the sample so that **H** was at various tilt angles θ_a toward the UTe_2 *a* axis. Figure S1 is an illustration of θ_a and θ_{bc} with respect to the crystal axes. An example dataset for $\theta_{bc} = 40°$ is shown in Fig. 1C. A high-field zero resistance state is obtained when **H** is applied within the *bc* plane ($\theta_a = 0°$). As **H** is tilted toward *a*, the field window in which superconductivity is observed shrinks until it is lost entirely around $\theta_a = 12.6°$. For $\theta_a \geq 12.6°$, the resistance instead shows a sharp increase, which is a signature of the metamagnetic transition (*17*).

Some samples were measured using a contactless conductivity technique: proximity detector oscillator (PDO) measurements (*18*). UTe_2's low electrical resistivity and challenging surface chemistry can make traditional electrical resistivity measurements difficult, especially in pulsed field. PDO experiments circumvent these technical obstacles and are a well-established technique for determining phase boundaries in UTe_2 and other superconductors (*2*, *19*–*22*). At 0.64 K, substantial shifts in PDO frequency *f* are seen at 8 and 45 T (Fig. 1D). Higher *f* is associated with lower resistance; for UTe_2, it has been established that the sudden rise in *f* as a function of field corresponds to the onset of a superconducting state, and that the subsequent decrease in *f* is the return to a resistive state (*2*). As temperature is increased, the superconducting phase boundaries shift in the expected fashion, and at 2.09 K, superconductivity is no longer observed. Instead, a kink downward is observed at 45 T, indicating a transition to a high-resistance FP phase. The metamagnetic transition field is labeled H_m. An extended discussion of PDO data analysis is provided in (*23*).

Angle-dependent phase diagrams

Figure 2 displays a set of field pulses and corresponding phase diagrams measured at three different θ_{bc} values. The core finding of this experiment is immediately apparent: As θ_{bc} decreases (i.e., the measurement plane moves closer to the *ab* plane), the effect of tilting toward *a* changes substantially. For $\theta_{bc} = 30°$ (Fig. 2A), increasing θ_a initially causes an enhancement of superconductivity instead of the immediate suppression seen in Fig. 1C. As θ_a is increased further, the critical field peaks around 60 T and then decreases until superconductivity is lost entirely around 15.5°, leaving a U-shaped region of superconductivity. The lower boundary tracks the angular evolution of H_m because SC_{FP} only exists within the FP phase.

At $\theta_{bc} = 23°$ (Fig. 2B), no superconductivity is observed in the *bc* plane ($\theta_a = 0$). However, tilting **H** toward *a* by 10° induces superconductivity. Superconductivity persists up to $\theta_a = 16°$, beyond which a metamagnetic transition is again observed. Similar behavior is observed close to the *ab* rotational plane at $\theta_{bc} = 8°$ (Fig. 2C), except that the onset θ_a and superconducting onset field H_{SC}^{on} have been pushed even higher. This reveals a superconducting regime that only appears at 59 T and persists well above 73 T, judging by the behavior of *f* versus

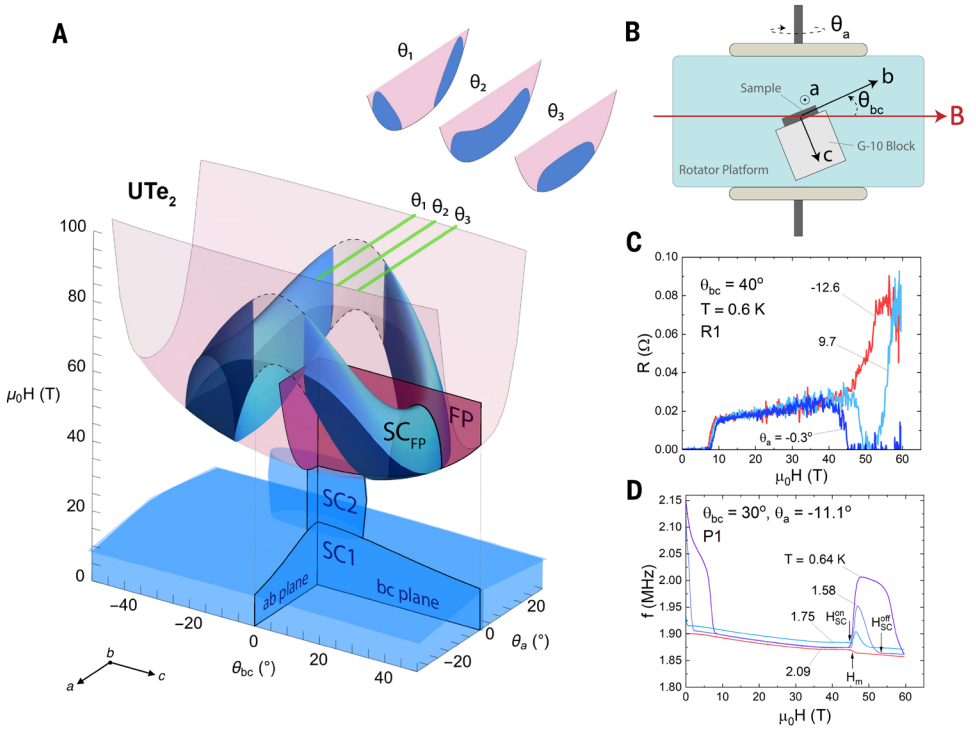

Fig. 1. Field-angle phase diagram of UTe_2 and experimental details. (**A**) Illustration of UTe_2's field-dependent phase diagram at 0.6 K, with the *ab* and *bc* planes highlighted. The three superconducting regions are shown in blue. The boundaries of the low-field SC1 phase vary smoothly with the field direction, whereas the field-stabilized SC2 phase exists only for fields near the *b* axis. The SC_{FP} state appears inside the field-polarized state (pink) only for specific off-axis fields that yield the saddle-like shape shown in the drawing. (**B**) Depiction of the measurement setup that enables effective dual-axis rotation. The crystal (gray) is placed on a block (white) on the rotator platform at a fixed angle within the *bc* plane (θ_{bc}), and the angle off of the *bc* plane (θ_a) is set to different values during the experiment. (**C**) Electrical resistance *R* versus field at various θ_a for sample R1 at ~0.6 K, revealing the high-field, zero-resistance SC_{FP} state. (**D**) Frequency of the proximity detector oscillator circuit as a function of applied field obtained at various temperatures for sample P1. An abrupt jump in *f* (indicating a transition to a low resistance state) is no longer observed at 2.09 K, consistent with a loss of superconductivity at that temperature.

H near the maximum field. The angular window of superconductivity also narrows noticeably at low θ_{bc}.

Figure 3A shows all of the phase diagrams measured in this experiment. This includes the PDO data presented in Fig. 2, as well as electrical resistance measurements performed on two additional samples. Consistent with the PDO data, in resistance measurements, an initial enhancement of the upper critical field (labeled H_{SC}^{off}) versus θ_a for the SC_{FP} phase is observed at $\theta_{bc} = 29°$, and the recovery of superconductivity by *a* axis tilting is seen at $\theta_{bc} = 18°$. The dimensions, critical temperature, and residual resistivity ratio of all four samples measured are given in table S1. Based on minor variations of the samples' critical temperatures, we expected some sample-dependent variations in the upper critical field, H_{SC}^{off}. In addition, higher-mass samples may experience greater field-induced heating, as discussed in (*24*), leading to a lower measured value of H_{SC}^{off} for higher-mass samples. Despite this, a coherent qualitative picture emerges. Stitching phase boundaries from these various θ_{bc} measurement planes together reveals the true structure of the SC_{FP} phase (illustrated in Fig. 1A). The region of superconductivity wraps around the *b* axis, with H_{SC}^{on} lowest within the *bc* plane and highest as **H** approaches the *ab* plane, reflecting the rapid increase of H_m with θ_a. This anisotropy is responsible for the saddle-like appearance in Fig. 1A.

Figure 3B shows a simpler picture that captures the primary revelation of this experiment. Here, we ignore *H* and plot the θ_{bc} and θ_a values at which an SC_{FP} phase is observed as closed points and the values where only H_m is seen as open circles. For easier visualization, the data have been symmetrized to fill all four quadrants, consistent with UTe_2's lattice symmetry and the absence of any observable difference between positive and negative field tilt angles. Blue shading is added as a guide to the eye because there is some slight scatter in the angular phase boundaries caused by sample dependence, angle uncertainty, and differing measurement techniques. Although we did not observe superconductivity within the *ab* plane, it is distinctly possible that H_{SC}^{on} in that plane exceeds the 73 T maximum field of the experiment. Additional details of the *ab* plane measurements are shown in fig. S8 and discussed in (*23*). Regardless of whether the SC_{FP} state truly does extend to the *ab* plane, the curvature of the phase boundaries is unambiguous, leading to the conclusion that a finite tilt of **H** off of *b* is what ultimately produces this unprecedented extreme high-field superconducting state. This contrasts with earlier inferences that a particular field direction within the *bc* plane is required. The onset angle off of *b* for superconductivity seems to be ~20°, or alternatively a perpendicular field $H_\perp$ of ~17 T, with some weak dependence on direction and sample characteristics.

Modeling the phase diagram

Despite the apparent similarities between θ_a and θ_{bc} in their relation to superconductivity, the two directions are crystallographically distinct. This anisotropy is apparent in the angular evolution of the FP phase boundaries (*2*), and understanding its interplay with the superconducting halo will be key for identifying the pairing mechanism and order parameter. The FP phase boundary, which serves as a lower bound for SC_{FP}, shifts to higher fields with increasing θ_a or θ_{bc}. We found that the field at which the metamagnetic transition occurs, H_m, can be modeled as a simple function of θ_{bc} and θ_a:

$$H_m = \frac{H_m^b}{\cos(\theta_{bc})} + \alpha_2 \sin^2\theta_a + \alpha_4 \sin^4\theta_a \quad (1)$$

where α_2 and α_4 are constants. Within the *bc* plane, H_m follows $H_m = H_m^b / \cos(\theta_{bc})$ where $H_m^b = 34$ T represents a typical value of H_m for $\mathbf{H} \parallel b$ (*2*, *25*). In other words, the metamagnetic transition occurs when $H_b = 34$ T regardless of H_c. However, when **H** is tilted outside of the *bc* plane, H_m shows a much steeper angle dependence on θ_a. Below the metamagnetic transition, *a* is the easy magnetic axis; tilts of field toward *a* oppose the spin reorientation at H_m, so it is reasonable that such tilts push the metamagnetic transition to higher fields.

Fitting the individual $H_m(\theta_a)$ curves to Eq. 1 yields two key findings. First, the function describes the data well. Second, the fitting parameters α_2 and α_4 are independent of θ_{bc}. The only parameter that varies is the *bc*-plane onset field $H_m^0 \equiv H_m^b / \cos(\theta_{bc})$. This point is illustrated in Fig. 3C: $H_m - H_m^0$ versus θ_a is plotted for all fixed θ_{bc} datasets, and all of the data collapse on top of each other. Fitting all phase boundaries together yields approximate values: $\alpha_2 = 95$ T and $\alpha_4 = 1934$ T. This

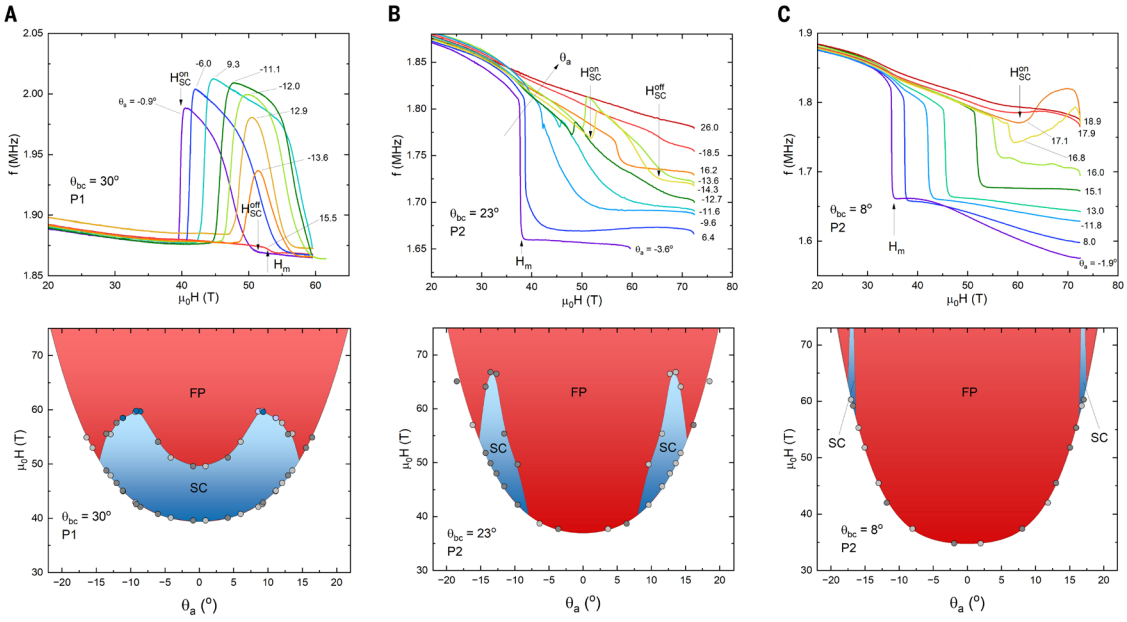

Fig. 2. Angle-dependent PDO data and corresponding phase diagrams. (**A** to **C**) Frequency of the proximity detector oscillator circuit versus magnetic field and corresponding phase diagrams collected at $\theta_{bc} = 30°$ for sample P1 (A), $\theta_{bc} = 23°$ for sample P2 (B), and $\theta_{bc} = 8°$ for sample P2 (C). All data in this figure were taken at ~0.6 K. An abrupt increase in *f* indicates a superconducting transition, whereas a decrease indicates a metamagnetic transition into the field-polarized phase. Superconducting regions are colored blue, and the electrically resistive portions of the field-polarized state are colored red. Darker points indicate θ_a values at which pulses were performed. Light points have been added at the corresponding $-\theta_a$ for clarity; this mirroring is justified by the underlying crystal symmetry. The blue points in the phase diagram of (A) indicate that the phase transition itself was above the measured field range and was identified through extrapolation (*23*).

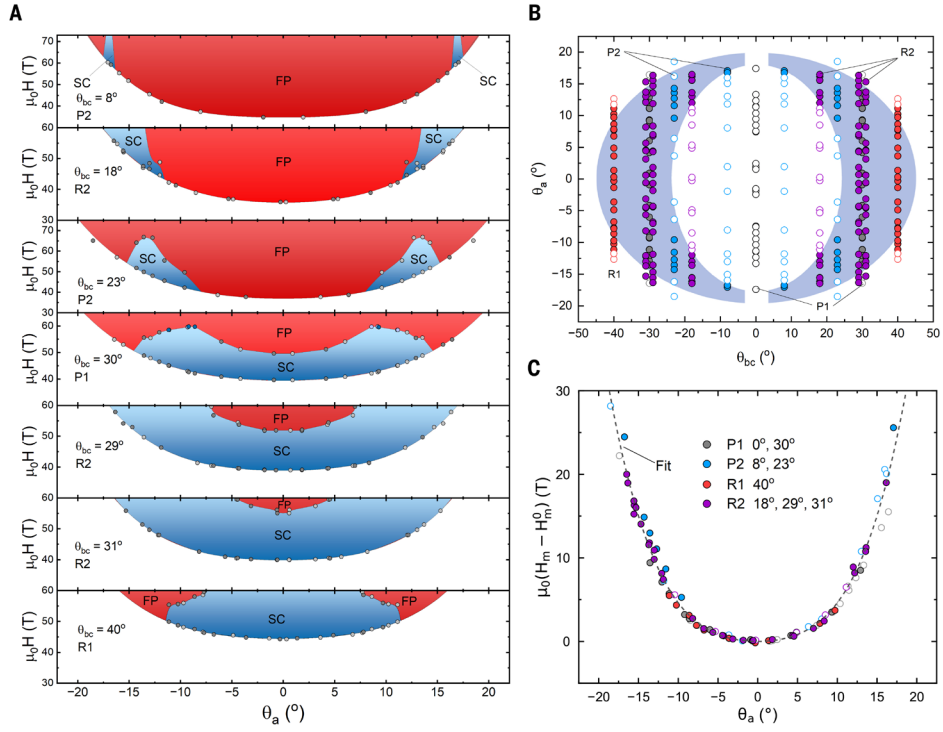

Fig. 3. Halo geometry of SC_{FP} state. (**A**) High-field phase diagrams presented as a function of θ_a collected at fixed θ_{bc} at ~0.6 K. Red indicates resistive regions of the FP phase, and blue indicates superconducting regions. The gray points represent the measured phase boundaries from which the plots are constructed, with the dark (light) points corresponding to actual (symmetrized) data. (**B**) Pure angular (θ_{bc} versus θ_a) representation of the superconducting phase boundaries at ~0.6 K. Full circles are used for angles at which superconductivity is observed, and open circles indicate that only a metamagnetic transition is seen. Different colors indicate different samples, as indicated in the figure. Data are symmetrized to populate all four quadrants for clarity. The blue halo is for illustrative purposes to emphasize that superconductivity is caused by tilting **H** off of *b*. (**C**) Measured transition field minus $H_m^0(\theta_{bc})$ at ~0.6 K plotted as a function of θ_a. As above, full circles indicate a superconducting transition and open circles indicate that only a metamagnetic transition is seen. For a given θ_{bc}, $H_m^0(\theta_{bc})$ is the metamagnetic transition field at $\theta_a = 0$. The legend indicates which colors are used for which sample and the θ_{bc} values at which data were collected. The dotted line is a fit of the entire data set to Eq.1 after subtracting off the individual $H_m^0(\theta_{bc})$ values.

scaling consistency indicates that tilts toward *a* and *c* have orthogonal effects on the FP phase, in contrast to their effects on the superconducting phase.

The survival of the SC_{FP} state to fields higher than 73 T indicates that the phase must be robust against spin-based depairing in addition to orbital depairing. The suggestion that SC_{FP} may be spin singlet with Jaccarino-Peter compensation at play (*26*) seems unlikely given our results showing an extended arc of field angles at which SC_{FP} occurs. It would require internal exchange fields that rotate smoothly and evolve similarly for fields tilting toward the *a* and *c* axes despite the magnetic anisotropy of UTe_2. The most natural explanation for our results is a triplet-pairing state, particularly given the evidence for spin-triplet superconductivity in the low-field state of UTe_2 (*4*).

Given that the SC_{FP} phase only arises within the FP state and not in the paramagnetic state of UTe_2, magnetic fluctuations likely play a

role in mediating the superconducting pairing. Whereas *b* is the magnetic hard axis at low fields, it becomes the magnetic easy axis in the FP phase (*27*). In this context, the fact that the superconducting halo surrounds the *b* axis also indicates the likely role of magnetism, possibly in the form of fluctuations that are enhanced by a finite transverse field. However, the specific interactions are not understood. Superconductivity in other uranium-based superconductors is often attributed to ferromagnetic spin fluctuations (*14*, *15*). This exact phenomenology cannot be applied to UTe_2 because UTe_2 is not a spontaneous ferromagnet and the SC_{FP} phase is not obviously linked with a second-order phase transition that would provide enhanced spin fluctuations. It is clear that there is no readily applicable existing theory for the behavior of the SC_{FP} phase.

Agnostic of the underlying pairing mechanism, we can model the phase diagram of SC_{FP} phenomenologically and calculate the angle dependence of the upper critical field. Our main conclusion is that the observed angle dependence of the upper critical field is most naturally explained if the Cooper pairs carry a finite spin $\mathbf{S}$ and/or orbital momentum $\mathbf{m}$:

$$\mathbf{S} = \int_{\mathrm{FS}} \frac{d^2k}{(2\pi)^2} \left(i\vec{d}_{\mathbf{k}} \times \vec{d}^{\,*}_{\mathbf{k}} \right), \mathbf{m}_{\mathrm{orb}} = \int_{\mathrm{FS}} d^2k \; i\vec{d}^{\,*}_{\mathbf{k}} \cdot \left[\mathbf{k} \times \boldsymbol{\partial}_{\mathbf{k}} \right] \vec{d}_{\mathbf{k}} \qquad (2)$$

where $\vec{d}_{\mathbf{k}}$ is the so-called *d* vector associated with the spin-triplet order parameter, which is a function of wavevector $\mathbf{k}$. When the resulting angular momentum, averaged over the Fermi surface, is nonvanishing, it will couple linearly to the magnetic field $\mathbf{B}$, yielding a term in the free energy of the form $\Delta F \propto -\mathbf{B} \cdot (\mathbf{S} + \mathbf{m}_{\mathrm{orb}})$. This term naturally depends on the field angle, as seen in the experiment.

A nonzero spin of the Cooper pairs in particular requires the order parameter to be multicomponent and nonunitary, the latter condition reflecting the fact that the norm of the order parameter $|\Delta(\mathbf{k})|^2 \propto |\vec{d}_{\mathbf{k}}|^2 \mathbf{1} + \mathbf{S} \cdot \sigma$ is not proportional to the identity matrix. As further discussed in (*28*), the order parameter for fields in the *bc* plane is likely $B_{2u} + iB_{3u}$, which has $\mathbf{S}$ and $\mathbf{m}_{\mathrm{orb}}$ both aligned along the *c* axis. As the field is tilted away from the *bc* plane, a B_{1u} component can appear in the order parameter, endowing the Cooper pairs with a component of the angular momentum along the *a* axis. This is natural to expect because the free energy is lowered when angular momentum acquires a component along the field direction. The theoretical analysis in (*28*) shows that this combination of order parameters qualitatively accounts for the halo shape of the superconducting region. For the D_{2h} point group to which UTe_2 belongs, the order parameters B_{1u}, B_{2u}, and B_{3u} correspond to nodal gap structures with point nodes along the *c*, *b*, and *a* axes, respectively.

Discussion and outlook

In summary, a 3D mapping of SC_{FP}'s angular phase boundaries unveils a superconducting state that appears only for fields tilted off of UTe_2's *b* axis and persists beyond 73 T. Known mechanisms of field-induced superconductivity fail to capture the nontrivial angle dependence uncovered in this work, and our theoretical analysis points to the key importance of the Cooper pairs having an angular momentum that couples to the external magnetic field. This would constrain the order parameter to be a multicomponent spin-triplet state. Our discovery provides an important direction for ultimately understanding the fundamental physics underpinning extreme high-field superconductivity.

REFERENCES AND NOTES

1. S. Ran *et al.*, *Science* **365**, 684–687 (2019).
2. S. Ran *et al.*, *Nat. Phys.* **15**, 1250–1254 (2019).
3. S. K. Lewin, C. E. Frank, S. Ran, J. Paglione, N. P. Butch, *Rep. Prog. Phys.* **86**, 114501 (2023).
4. D. Aoki *et al.*, *J. Phys. Condens. Matter* **34**, 243002 (2022).
5. L. Jiao *et al.*, *Nature* **579**, 523–527 (2020).
6. I. M. Hayes *et al.*, *Science* **373**, 797–801 (2021).
7. G. Knebel *et al.*, *J. Phys. Soc. Jpn.* **88**, 063707 (2019).
8. H. Sakai *et al.*, *Phys. Rev. Mater.* **6**, 073401 (2022).
9. Y. S. Eo *et al.*, *Phys. Rev. B* **106**, L060505 (2022).
10. T. Thebault *et al.*, *Phys. Rev. B* **106**, 144406 (2022).
11. J. M. Lu *et al.*, *Science* **350**, 1353–1357 (2015).
12. J. Singleton, C. Mielke, *Contemp. Phys.* **43**, 63–96 (2002).
13. L. Balicas *et al.*, *Phys. Rev. Lett.* **87**, 067002 (2001).
14. D. Aoki, K. Ishida, J. Flouquet, *J. Phys. Soc. Jpn.* **88**, 022001 (2019).
15. F. Lévy, I. Sheikin, B. Grenier, A. D. Huxley, *Science* **309**, 1343–1346 (2005).
16. W. Knafo *et al.*, *Commun. Phys.* **4**, 40 (2021).
17. W. Knafo *et al.*, *J. Phys. Soc. Jpn.* **88**, 063705 (2019).
18. M. M. Altarawneh, C. H. Mielke, J. S. Brooks, *Rev. Sci. Instrum.* **80**, 066104 (2009).
19. Z. Wu *et al.*, *Proc. Natl. Acad. Sci. U.S.A.* **121**, e2403067121 (2024).
20. S. E. Sebastian, N. Harrison, G. G. Lonzarich, *Rep. Prog. Phys.* **75**, 102501 (2012).
21. M. Nikolo *et al.*, *J. Supercond. Nov. Magn.* **30**, 561–568 (2017).
22. M. Smylie *et al.*, *Phys. Rev. B* **100**, 054507 (2019).
23. See the supplementary text.
24. See the materials and methods, "Experimental information" section.
25. C. E. Frank *et al.*, *Nat. Commun.* **15**, 3378 (2024).
26. T. Helm *et al.*, *Nat. Commun.* **15**, 37 (2024).
27. A. Miyake *et al.*, *J. Phys. Soc. Jpn.* **88**, 063706 (2019).
28. See the materials and methods, "Theoretical modeling of H_{c2}" section.
29. S. K. Lewin, P. Czajka, Data for: High-field superconducting halo in UTe_2, version 2.0, Harvard Dataverse (2024); https://doi.org/10.7910/DVN/EYNSUX.

ACKNOWLEDGMENTS

We thank D. Agterberg for helpful discussions. Identification of commercial equipment does not imply recommendation or endorsement by NIST. **Funding:** Crystal synthesis and characterization, sample preparation, and high-field measurements were supported by the National Science Foundation under Division of Materials Research Grant NSF-DMR 2105191. A portion of this work was performed at the National High Magnetic Field Laboratory (NHMFL), which is supported by National Science Foundation Cooperative Agreements DMR-1644779 and DMR-2128556, the state of Florida, and the US Department of Energy (DOE). Electrical contact preparation was supported by DOE Award DE-SC-0019154. The theoretical analysis by A.H.N. was supported by the DOE, Office of Basic Energy Sciences (BES), under Award DE-SC0025047. J.P. was supported by the Gordon and Betty Moore Foundation's EPiQS Initiative through Grant GBMF9071. J.S. was supported by the DOE BES program "Science of 100 T," which permitted the design and construction of much of the specialized equipment used in the high-field studies. **Author contributions:** S.K.L., P.C., and N.P.B. conceived of and designed the study. C.E.F. synthesized the samples. S.K.L., P.C., C.E.F., and G.S.S. prepared and characterized the samples. Y.S.E., H.Y., and J.P. assisted with the preparation of electrical leads. S.K.L., P.C., G.T.N., and J.S. performed the pulsed field experiments. A.H.N. performed theoretical analysis. S.K.L., P.C., and N.P.B. prepared the manuscript with input from all authors. **Competing interests:** The authors declare no competing interests. **Data and materials availability:** The data from this study are publicly accessible through the Harvard Dataverse (*29*).

SUPPLEMENTARY MATERIALS

science.org/doi/10.1126/science.adn7673
Materials and Methods; Supplementary Text; Figs. S1 to S10; Table S1; References (*30*–*34*)

Submitted 21 March 2024; accepted 5 June 2025

10.1126/science.adn7673